Dalton Transactions

ROYAL SOCIETY OF CHEMISTRY

PAPER

View Article Online
View Journal | View Issue

Cite this: *Dalton Trans.*, 2026, **55**, 2883

The influence of the coordination environment of cobalt(II) ions on the magnetic properties of heterometallic complexes with a $\{Co_2Li_2\}$ metal core

Irina K. Rubtsova, *[a] Dmitriy S. Yambulatov, [a] Maxim A. Shmelev, [a] Julia K. Voronina, [a] Alexander S. Goloveshkin, [b] Konstantin A. Babeshkin, [a] Nikolay N. Efimov, [a] Anna K. Matiukhina, [a] Stanislav A. Nikolaevskii, *[a] Mikhail A. Kiskin [a] and Igor L. Eremenko [a]

Received 24th October 2025,
Accepted 13th January 2026

DOI: 10.1039/d5dt02560e

rsc.li/dalton

Five new heterometallic carboxylate complexes of the composition $[Co_2Li_2(A)_6(L)_2]$ (L = 4-phenylpyridine, A = 2-furoate anion (**1**); L = 2,2′-bipyridine, A = 2-furoate anion (**2**), 3,5-di-*tert*-butylbenzoate anion (**3**); L = quinoline, A = 3-cyanobenzoate anion (**4**), 4-cyanobenzoate anion (**5**)) were synthesized. The structures of all compounds were determined by single-crystal X-ray diffraction. When monodentate N-donor ligands are replaced by chelating 2,2′-bipyridine, the coordination polyhedron of cobalt ions changes from a distorted tetrahedron to a distorted octahedron. Complexes **1–4** are field induced single-molecule magnets. Mechanisms of slow magnetic relaxation are discussed taking into account both experimental data and quantum chemical calculations.

Introduction

The directed design of new substances exhibiting magnetic ordering at the molecular level is one of the most topical directions in modern coordination chemistry.[1–7] The interest in single-molecule magnets (SMMs) is due to their potential application in information recording, storage and processing, quantum computing, and spintronics.[8–11]

From the row of transition metals, cobalt is the most promising element for the directed synthesis of coordination compounds exhibiting SMM properties.[12,13] Co(II) is a Kramers ion (has a half-integer spin) and possesses high magnetic anisotropy tuned by the local coordination environment. This fundamental property, along with the high spin value, allows SMMs based on Co(II) ions to show high values of U_{eff}.

Amidst SMMs based on cobalt complexes, three compounds have shown record performance.[10,14,15] Among them, only the complex $[Co(PzOx)_3(BC_6H_5)]Cl$ (U_{eff} = 152 cm^{-1} (219 K); PzOx is the tris-pyrazoloximate ligand), in which the cobalt atom is in a trigonal prismatic environment, is resistant to environmental factors. Compounds [(sIPr)Co(NDmp)] (U_{eff} = 413 cm^{-1} (594 K); sIPr is 1,3-bis(2,6-diisopropylphenyl)imidazol-2-ylidine, Dmp is 2,6-dimesitylphenyl) and $[Co(C(SiMe_2ONaph)_3)_2]$ (U_{eff} = 450 cm^{-1} (648 K); Naph is naphthyl) are two-coordinated cobalt complexes and are very sensitive to air and moisture. The latter drawback is common to all cobalt complexes with a coordination number of 2.[16–19] The challenge of creating stable complexes with SMM behavior and high operational performance remains relevant.

Owing to a wide range of coordination modes, carboxylate ligands allow the synthesis of metal complexes of diverse structural types. Directed regulation of the structural features of complexes, particularly by variation of the substituent at the carboxyl group, allows the physicochemical properties of the target compounds to be fine-tuned.[20–26]

Carboxylate complexes of Co(II) are a quite promising group of compounds in the context of the search for new SMMs. To our knowledge, Co(II) carboxylates are mainly field-induced SMMs, and creation of zero-field magnets based on this class of complexes still remains a challenging task. Nevertheless, synthetic availability and high stability of Co(II) carboxylates motivate investigators to obtain new compounds of such type and to study their magnetic properties. Remarkable results in Co(II) carboxylate based SMMs are associated with achievements in the synthesis of multinuclear Co(II) cuban-type complexes based on acetate and citrate ligands. These complexes have U_{eff} = 10.4 cm^{-1} (15 K) and 15 cm^{-1} (21 K) at H_{DC} of 1000

[a]*N.S. Kurnakov Institute of General and Inorganic Chemistry, Russian Academy of Sciences, Leninsky prosp. 31, 119991 Moscow, Russian Federation. E-mail: irina.k.rubtsova@gmail.com, sanikol@igic.ras.ru*

[b]*A.N. Nesmeyanov Institute of Organoelement Compounds, Russian Academy of Sciences, Vavilova Str. 28, 119991 Moscow, Russian Federation*

Oe for $[Co_{12}(bm)_{12}(NO_3)(O_2CMe)_6(EtOH)_6](NO_3)_5$ (bm is deprotonated (1*H*-benzimidazol-2-yl)methanol) and $(C(NH_2)_3)_8[Co_4(cit)_4]\cdot 4H_2O$ (cit is the citrate trianion), respectively.[27,28] More recently, a series of Co(II)–Y(III) carboxylates (acetate, trichloroacetate, pivalate and benzoate) with a large positive *D* value was studied. Slow magnetic relaxation was approximated by the combination of Raman, direct, and QTM mechanisms.[29]

Heterometallic carboxylate complexes are promising objects for the design of magnetic materials.[30–36] Directed assembly of heterometallic complexes using bridging carboxylate ligands and ancillary N-donor ligands, blocking the formation of coordination polymers, is one of the most convenient and frequently used methods for synthesizing polynuclear compounds.[37–40]

Heterometallic complexes containing both 3d-metal and lithium cations can be promising systems for the design of SMMs because diamagnetic lithium cations allow the separation of paramagnetic 3d-metal cations in space, which can positively affect the efficiency of the corresponding SMMs under certain conditions.[41] Note that diamagnetic dilution is one of the effective tools to suppress quantum tunneling of magnetization (QTM).[42–45] Another way to influence the contribution of QTM to relaxation processes is to control the packing of molecules in the crystal. Significant distancing of metal centers from each other can be achieved by using bulky ligands, thereby minimizing intermolecular exchange interactions and QTM.[46–48]

Previously, we reported compounds $[Co_2Li_2(piv)_6(IMes)_2]$, $[Co_2Li_2(piv)_6(Ph_3P)_2]$, $[Co_2Li_2(2\text{-fur})_6(py)_2]$, $[Co_2Li_2(piv)_6(4\text{-}MeOC_6H_4\text{-MIAN})_2]$ and $(HI\mathit{t}Bu)_2[Co_2Li_2(\mu^2\text{-piv})_6(\kappa^1\text{-piv})_2]$ (piv is the pivalate anion, IMes is 1,3-bis-(2,4,6-trimethylphenyl)imidazol-2-ylidene, py is pyridine, 4-$MeOC_6H_4$-MIAN is *N*-(4-methoxyphenyl)-mono-iminoacenaphthenone, HI*t*Bu is protonated 1,3-di-*tert*-butylimidazol-2-ylidene) with a positive *D* value. They demonstrated relaxation described by the sum of the Raman mechanism and the direct process.[49–51] In these tetranuclear complexes the $\{Co_2Li_2\}$ metal core is very stable, which implies the possibility of quite easy variation of carboxylate anions and ancillary terminal ligands. The use of these factors makes it possible to tune both the parameters of the coordination environment of Co(II) atoms and to regulate intermolecular interactions using carboxylate anions with different degrees of steric hindrance. At the same time, the electronic effects of the substituents in both carboxylate anions and neutral ancillary ligands can influence the magnetic properties of the discussed compounds.

Herein, we describe the synthesis, structure and magnetic properties of five new heterometallic complexes of the composition $[Co_2Li_2(A)_6(L)_2]$ (A = anions of 2-furoic acid (2-fur), 3,5-di-*tert*-butylbenzoic acid (bzo), 3-cyanobenzoic acid (3-cba), 4-cyanobenzoic acid (4-cba); L = 4-phenylpyridine (4PhPy), 2,2′-bipyridine (bpy), and quinoline (quin)). We varied both carboxylic acid anions and N-donor ligands within this series of compounds, including their spatial and electronic structure characteristics.

Results and discussion

Complexes **1–5** were synthesized by reaction of cobalt pivalate, lithium pivalate, three equivalents of the corresponding carboxylic acid and N-donor ancillary ligand in acetonitrile (Scheme 1). All compounds were isolated as single crystals and polycrystalline samples. The composition of the compounds is confirmed from elemental analysis data.

Single crystal X-ray diffraction

All synthesized complexes have a similar structure and contain a tetranuclear $\{Co_2Li_2\}$ metal core, in which cobalt atoms are linked with lithium atoms *via* three bridging carboxylate groups (compounds **1**, **4**, and **5**) or one chelate-bridging and two bridging carboxylate groups (compounds **2** and **3**). In all complexes, each Li atom coordinates four oxygen atoms of three carboxylate groups, which connect it with the Co atom and one adjacent $\{CoLi(O_2CR)_3\}$ fragment with the formation of a tetranuclear $\{Co_2Li_2\}$ metal core. All metal atoms lie in the same plane. In all compounds, Li atoms are in a distorted tetrahedral environment. The main crystallographic parameters and details of structure refinement of **1–5** are given in Table S1.

Complex **1** crystallizes in the space group $P2_1/c$ with the inversion center at the intersection of the diagonals of the O_2Li_2 fragment. In structure **1**, each Co ion coordinates three O atoms of bridging furoate groups and one N atom of the 4-phenylpyridine molecule with formation of a distorted tetrahedral environment ($S_Q(CoNO_3) = 0.875$) (Fig. 1).

Complex **2** crystallizes in the space group $P\bar{1}$ with the inversion center at the intersection of the diagonals of the O_2Li_2

$$[\mathbf{Co}(piv)_2]_n + [\mathbf{Li}(piv)]_n + 3\ HA + L \xrightarrow{CH_3CN} [\mathbf{Co_2Li_2}(A)_6(L)_2]$$

HA = 2-Hfur, L = 4PhPy (**1**)
HA = 2-Hfur (**2**), Hbzo (**3**), L = bpy
HA = 3-Hcba (**4**), 4-Hcba (**5**), L = quin

Scheme 1 Synthesis of complexes **1–5**.

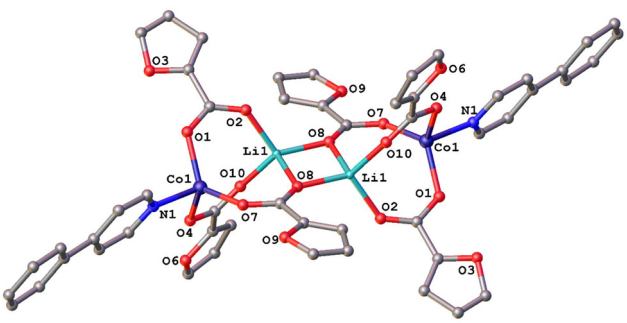

Fig. 1 Structure of complex **1**. Hydrogen atoms are not shown for clarity.

fragment. The replacement of the 4-phenylpyridine by 2,2′-bipyridine in the case of compound **2** leads to the transition of the bridging furoate groups, which bind Co and Li ions, to a chelate-bridging type of coordination, as well as the decrease in the Co...Li distance and the extension of the Li...Li distance (Fig. 2 and Table 1), compared with complex **1**. In structure **2** each Co atom coordinates four O atoms of one chelate-bridging and two bridging furoate anions and two N atoms of the 2,2′-bipyridine molecule. The coordination polyhedron of the cobalt atom is a distorted octahedron ($S_Q(CoN_2O_4)$ = 2.814).

Complex **3** crystallizes in the space group $P2_1/c$. The replacement of the furoate groups by 3,5-di-*tert*-butyl-benzoate groups does not lead to the significant change of the geometry of the complex; metal cores in **2** and **3** have a similar structure (Fig. S1). When comparing the geometric parameters of complexes **2** and **3**, it is possible to note only the decrease of the Li...Li distance by 0.18 Å and the increase in the value of the Li–Li–Co angle by 4 degrees in the case of complex **3**. The main bond lengths and the Co...Li distance have similar values in complexes **2** and **3** (Table 1). The coordination environment of the terminal cobalt atoms in **3** is a distorted octahedron ($S_Q(CoN_2O_4)$ = 3.082).

Complexes **4** and **5** crystallize in the space groups $P\bar{1}$ and $P2_1/c$, respectively. Similar to compound **1**, the cobalt ions in **4** and **5** have a distorted tetrahedral environment ($S_Q(CoNO_3)$ = 0.888 for **4** and $S_Q(CoNO_3)$ = 0.930 for **5**), which is formed as a result of coordination of three O atoms of cyanobenzoate groups and the N atom of the quinoline molecule (Fig. 3 and Fig. S2). The replacement of 3-cyanobenzoate by the 4-cyanobenzoate group does not significantly affect the geometry of the complexes; their metal cores have an analogous structure.

In the crystal packings of complexes **1–3**, the formation of intermolecular stacking interactions between the pairs of N-donor ligands is observed, which leads to the formation of supramolecular chains (Fig. S3–S5 and Table S2). In the case of compounds **4** and **5**, the formation of stacking interactions between the pairs of 3-cyanobenzoate or 4-cyanobenzoate groups is observed (Fig. S6 and Table S2). In complex **5**, additional formation of intermolecular interactions between the 4-cyanobenzoate groups and quinoline molecules is observed (Fig. S7 and Table S2). Also, crystal packings of all obtained compounds are stabilized by C–H···O interactions

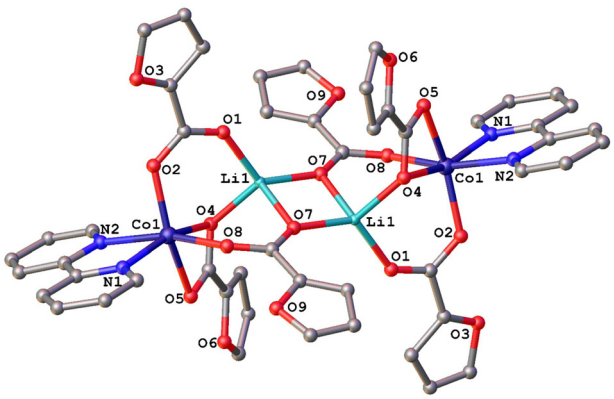

Fig. 2 Structure of complex **2**. Hydrogen atoms are not shown for clarity.

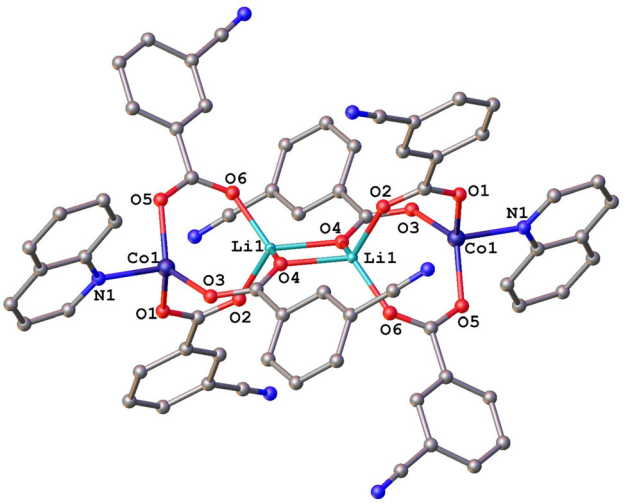

Fig. 3 Structure of complex **4**. Hydrogen atoms are not shown for clarity.

Table 1 Main bond lengths, interatomic distances and angles in the structures of complexes **1–5**

	Length, Å				
Bond	**1**	**2**	**3**	**4**	**5**
Co–O	1.944(3)–1.957(3)	2.019(2)–2.288(2)	2.010(3)–2.266(3)	1.949(6)–1.979(6)	1.947(7)–1.960(7)
Co–N	2.066(8), 2.072(8)	2.108(2), 2.142(2)	2.114(4), 2.131(3)	2.048(7)	2.063(8)
Li–O	1.875(7)–1.977(7)	1.916(4)–1.984(5)	1.858(9)–1.950(9)	1.868(15)–1.968(15)	1.803(17)–1.946(17)
Co...Li	3.173(6)	3.137(3)	3.104(7)	3.186(14)	3.158(14)
Li...Li	2.742(12)	2.817(8)	2.644(16)	2.80(3)	2.692(3)
Co...Co	8.110(1)	8.138(1)	8.073(1)	8.075(7)	8.038(6)
Angle, ω/deg					
Li–Li–Co	121.1(3)	122.3(2)	126.7(4)	118.1(9)	120.9(8)

between the hydrogen atoms of organic ligands and the oxygen atoms of carboxylate groups or furoic cycles in the case of complexes **1** and **2** (Table S3). For compounds **4** and **5**, the formation of additional C–H···N interactions involving the cyano groups of 3- and 4-cyanobenzoate groups is observed. In the case of compound **4** with 3-cyanobenzoate groups, intermolecular C–N...π interactions are also formed between the cyano group of the 3-cyanobenzoate group and quinoline molecule (Table S4), whereas in the case of compound **5** with the 4-cyanobenzoate group, similar interactions are not observed.

The phase purity of the obtained complexes **1–4** was confirmed by means of powder X-ray diffraction (Fig. S8–S11). In the case of compound **5**, we could not obtain a phase-pure sample.

DC-magnetic investigations

The dc magnetic susceptibility measurements of complexes **1–4** were carried out in the temperature range of 2–300 K under a dc-field of 5000 Oe. For all compounds, χT values at 300 K are significantly higher than the spin-only values for two non-interacting cobalt(II) ions (Table S5) which is probably due to the orbital contribution.

Moreover, for complexes **1** and **4** with a pseudo-tetrahedral coordination environment, smaller χT values at 300 K are characteristic, whereas for **2** and **3** values are higher due to a larger orbital contribution realized due to the pseudo-octahedral environment.[52,53] The course of the χT curves for **1** and **4** is monotonous up to 30 K, when both values reach 4.65 cm^3 K mol^{-1}, then a sharp drop is observed upon further cooling (Fig. 4). In the case of complexes **2** and **3**, the χT values decrease smoothly to 5.4 and 5.3 cm^3 K mol^{-1} at 80 K consequently, and then a sharp decrease in thermal susceptibility is observed (Fig. 4).

The M(H) and M(H/T) dependencies for compounds **1–4** were also measured at 2, 4, and 6 K (Fig. S12).

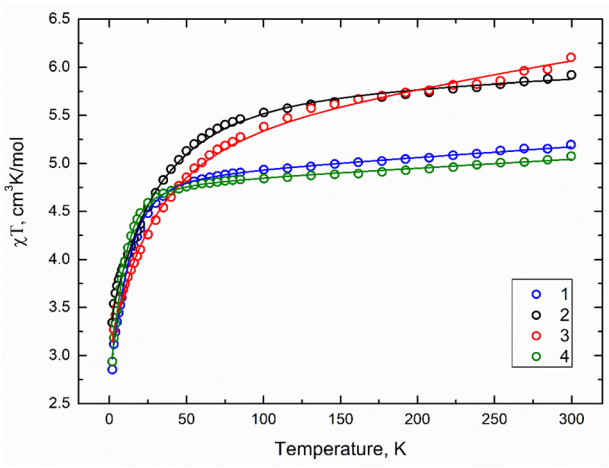

Fig. 4 Temperature dependencies χT of complexes **1–4** under a 5000 Oe dc magnetic field. The solid lines represent the best fit by the PHI program.[54]

Table 2 Experimental and theoretically calculated parameters of spin Hamiltonian

	1	2	3	4
Analysis of experimental data				
D, cm^{-1}	14.910	20.589	20.077	10.884
g_{iso}	2.274	2.468	2.379	2.255
TIP, cm^3 mol^{-1}	1.08×10^{-3}	6.53×10^{-4}	2.62×10^{-3}	9.23×10^{-4}
ZFS parameters and g values based on CASSCF/NEVPT2 calculations				
D, cm^{-1}	22.585	40.016	40.660	16.427
E/D	0.039	0.244	0.265	0.208
g_x	2.093	2.069	2.073	2.139
g_y	2.289	2.360	2.362	2.255
g_z	2.310	2.576	2.594	2.328

The experimental χT(T) and M(H) dependencies were approximated simultaneously using the PHI program[54] according to the spin Hamiltonian (eqn (1)).

$$\hat{H} = D\left[\hat{S}_z{}^2 - \frac{1}{3}S(S+1)\right] + \mu_B \vec{B} \cdot g_{iso} \cdot \hat{S} \quad (1)$$

where D – axial zero-field splitting parameter, $\hat{S}$ – spin momentum operator, S – total spin, g – g-factor, μ_B – Bohr magneton, and $\vec{B}$ – applied magnetic field.

The rhombic parameter E was not set to avoid over-parameterization. The best-fit values of D and g_{iso} are given in Table 2.

Quantum chemical calculations

To interpret the dc magnetic data, *ab initio* (post-HF) quantum chemical calculations were performed on the X-ray crystal structures of complexes. The spin-Hamiltonian parameters of individual centers were calculated using the complete active space self-consistent field theory (CASSCF) and the dynamic correlations were captured by performing N-electron valence second-order perturbation theory (NEVPT2).

For complexes **1** and **4**, the obtained ground state energies correspond to pseudo-tetrahedral Co(II) complexes with the C_{3v} point symmetry group.[55,56] In this case, the spherical term ^{4}F, when reduced to T_d symmetry, splits into $^4A_2$, $^4T_2$, and $^4T_1$, where term $^4A_2$ has the lowest energy. With further symmetry reduction to C_{3v}, the $^4T_2$ level splits into ^4E and $^4A_{2'}$, while the symmetry of the ground $^4A_2$ term remains unchanged.[55]

In the structure of the polyhedron in pseudo-octahedral complexes **2** and **3**, there are no clearly expressed axial and equatorial positions, and the point group corresponds to C_{2v}.[57,58] In the case of Co(II) complexes with O_h crystal field symmetry, the spherical term ^{4}F splits into $^4T_{1g}$, $^4T_{2g}$, and $^4A_{2g}$, with $^4T_{1g}$ being the ground state. Upon lowering the symmetry to D_{4h}, the $^4T_{1g}$ term splits into an orbital singlet $^4A_{2g}$ and a doublet ^4E_g. According to quantum chemical calculations, the ground spin-free state is the orbital singlet, which, upon further symmetry reduction to C_{2v}, transforms into the state $^4A_2$. Due to this, the orbital moment is largely quenched. The rhombic distortion leads to splitting of the excited orbital doublet ^4E_g into $^4B_1 \otimes {}^4B_2$ states,[58] exceeding 1000 cm^{-1} in energy (Table S6).

Thus, high-lying Kramers doublets arising from $^4B_1$ term splitting do not contribute to the anisotropy, and the classical spin Hamiltonian can be used for interpretation (eqn (2)).

$$\hat{H} = D\left[\hat{S}_z^2 - \frac{1}{3}S(S+1)\right] + E(\hat{S}_x^2 - \hat{S}_y^2) + \mu_B \vec{B} \cdot g \cdot \hat{S} \quad (2)$$

where D and E – axial and rhombic ZFS parameters, $\hat{S}$ – spin momentum operator, S – total spin, g – g-factor, μ_B – Bohr magneton, and $\vec{B}$ – applied magnetic field.

The calculated parameter values show an easy-plane type of anisotropy for all complexes (Table 2), but only compounds **2–4** exhibit a strong rhombic distortion of magnetic anisotropy, represented by the E/D ratio.

In complexes, the two low-lying Kramers doublets (KD^0, KD^I) formed as a result of spin–orbital interactions are well separated from the higher-lying ones, but are subject to significant wavefunctions mixing (Table S7). As a result, the energy of the first excited doublet (KD^I) exceeds the values of $2|D|$.

In an effort to have intricate details of slow magnetic relaxation phenomena, we have plotted the blocking barrier for complexes **1–4** computed using the SINGLE ANISO approach.[59] The calculated elements of the magnetic moment matrix indicate the presence of a significant contribution of the QTM (1.529, 0.784, 0.752 and 0.822μ_B for **1–4**, respectively), due to which slow relaxation is not observed in zero field (Fig. S13). When a magnetic field of 1000 Oe is applied, despite the easy-plane type of anisotropy of the complexes, the multideterminant character of spin–orbital states enables slow magnetic relaxation to be realized.

AC-magnetic investigations

In order to determine the presence of slow magnetic relaxation in complexes **1–4**, ac magnetic susceptibility measurements were carried out. The out-of-phase signal χ'' of complexes **1–4** in a zero dc-field is negligibly small compared to the in-phase signal χ' (Fig. S14). The application of an external dc-field reduces the probability of quantum tunneling of magnetization (QTM), which may lead to the possibility of observing slow magnetic relaxation in the system. Measurements of the ac magnetic susceptibility in non-zero dc magnetic fields resulted in the appearance of the significant signal on the out-of-phase frequency dependencies of the studied compounds. The variation of the external dc-field (H_{DC}) allowed us to determine the optimal value (1000 Oe), at which the maxima on the corresponding $\chi''(\nu)$ dependencies are located at the lowest frequency values, which corresponds to the longest relaxation times (Fig. S14), which corresponds to the case when the probability of relaxation by the QTM mechanism is minimal.

To determine the temperature dependence of the relaxation time in the optimal dc-field, measurements of the isotherms of the frequency dependencies of the ac magnetic susceptibility were carried out in the temperature range 2–3.75 K for **1**, 2–6 K for **2**, 2–5.25 K for **3**, and 2–3 K for **4** (Fig. S15). To produce the τ *vs.* $1/T$ plots, the out-of-phase component dependencies were approximated by the generalized Debye model (Fig. 5 and 6).

For all complexes, the high-temperature range of the dependence of the relaxation time on the inverse temperature $\tau(1/T)$ was

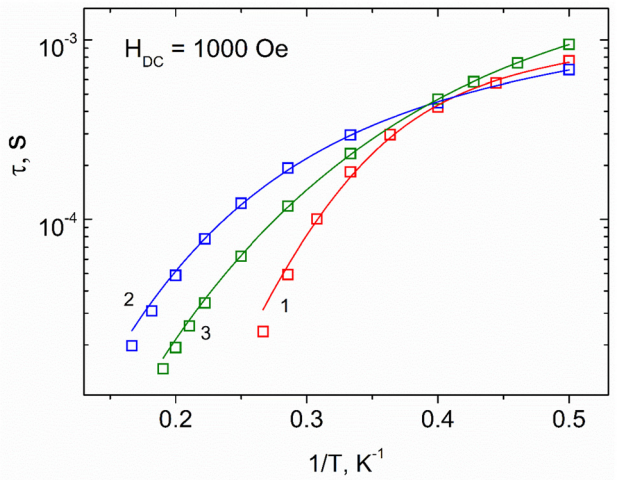

Fig. 5 The τ *vs.* $1/T$ plots for **1** (red), **2** (blue) and **3** (green) under the optimal dc-field of 1000 Oe. Solid lines represent fitting by the sum of the Raman and direct relaxation mechanisms.

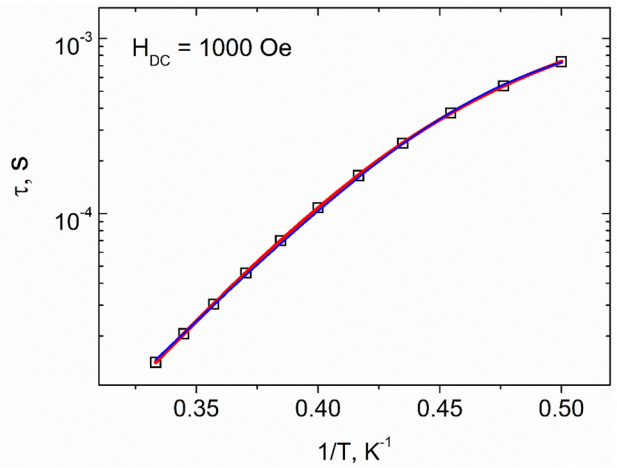

Fig. 6 The τ *vs.* $1/T$ plot for **4** under the optimal dc-field of 1000 Oe. The red solid line represents fitting by the sum of the Orbach, Raman and direct relaxation mechanisms. The blue solid line represents fitting by the sum of the vibrational process and direct mechanism.

approximated by the Arrhenius equation ($\tau = \tau_0 \exp(\Delta E/kT)$) (Orbach mechanism). The best-fit parameters are given in Table 3.

When approximating the high-temperature region with the Arrhenius equation, the barriers obtained are close to the calculated spin–orbital states only in the case of **4**. In the case of **1–3**, the Orbach mechanism is unrealizable, since the magnetization reorientation requires accessible phonons of the corresponding energy and a real level.[60,61] The most probable relaxation mechanism for **1–3** is a combination of the Raman and direct processes ($\tau^{-1} = C_{Ram}T^{n_{Ram}} + A_{dir}TH^4$) (Fig. 5). The best-fit parameters for **1–3** are given in Table 3. For more approximation details, see Tables S8–S10.

For complex **4**, in a semi-logarithmic coordinate system, the dependence of the relaxation time on the reciprocal tempera-

Table 3 The best-fit parameters of magnetization relaxation for **1–4** (H_{DC} = 1000 Oe)

		Complex			
		1	**2**	**3**	**4**
T, K (high-temperature range)		3.25–3.75	5–6	4.5–5.25	2.7–3
Orbach	$\Delta E/k$, K	33.79 ± 1.45	26.45 ± 1.10	26.20 ± 0.50	31.36 ± 0.29
	τ_0, s	$3.07 \times 10^{-9} \pm 1.38 \times 10^{-9}$	$2.47 \times 10^{-7} \pm 5.27 \times 10^{-8}$	$1.02 \times 10^{-7} \pm 1.10 \times 10^{-8}$	$4.14 \times 10^{-10} \pm 4.47 \times 10^{-11}$
T, K (whole temperature range)		2–3.75	2–6	2–5.25	2–3
Raman	C_{Ram}, s^{-1} $K^{-n_{Ram}}$	0.20 ± 0.01	9.71 ± 1.96	13.45 ± 0.87	Another combination of mechanisms (see the text)
	n_{Ram}	9 (fix)	4.62 ± 0.15	5.04 ± 0.06	
Direct	A_{dir}, K^{-1} Oe^{-4} s^{-1}	$6.15 \times 10^{-10} \pm 1.15 \times 10^{-11}$	$6.17 \times 10^{-10} \pm 1.46 \times 10^{-11}$	$3.09 \times 10^{-10} \pm 6.42 \times 10^{-12}$	
R^2		0.99756	0.99961	0.99996	

ture is linear within the temperature range of 2.7–3 K. This implies the possibility of magnetization relaxation *via* the Orbach mechanism. The best-fit parameter τ_0 value 4.14×10^{-10} s is characteristic for the Orbach mechanism, as it is in the range of 10^{-10}–10^{-12} s.[62] In the whole temperature range the best agreement of the theoretical curve with the experimental data for **4** was achieved by approximation by the sum of the Orbach, Raman and direct relaxation mechanisms ($\tau^{-1} = \tau_0^{-1}\exp(-\Delta E/kT) + C_{Ram}T^{n_{Ram}} + A_{dir}TH^4$) with the following parameters: $\Delta E/k$ = 34.43 ± 0.31 K, $\tau_0 = 1.64 \times 10^{-10} \pm 1.87 \times 10^{-11}$ s, C_{Ram} = 25.88 ± 1.01 s^{-1} $K^{-n_{Ram}}$, n_{Ram} = 5 (fix), $A_{dir} = 1.63 \times 10^{-10} \pm 1.28 \times 10^{-11}$ K^{-1} Oe^{-4} s^{-1}, R^2 = 1 (Fig. 6, red line). For more approximation details, see Table S11.

Strong mixing of spin–orbital states (Table S7), leading to the energy barrier in an applied field, could theoretically explain the Orbach process. When refining the relaxation dependence by sum of the Orbach, Raman and direct mechanisms without fixed values, the power-law value in the Raman mechanism is close to 4 (Table S11). The latter may be caused by whether contribution of acoustic phonons or the second-order Raman process occurring through a local vibrational frequency located below the spin–orbital state.[63–73] We assume that in our case the second pathway is more plausible.

An approximation including the vibrational process and direct mechanism (eqn (3)) with parameters ω = 31 K (21.5 cm^{-1}), $A_{loc} = 2.05 \times 10^9 \pm 3.26 \times 10^7$ s^{-1}, $A_{dir} = 4.93 \times 10^{-10} \pm 5.67 \times 10^{-12}$ K^{-1} Oe^{-4} s^{-1}, R^2 = 0.99967 is also possible for describing the relaxation process for complex **4** (Fig. 6, blue line). Similar values of the vibrational quantity were previously found, including for a wide series of Co^{2+} complexes.[74,75]

$$\tau^{-1} = A_{loc}\frac{e^{\frac{-\omega}{kT}}}{\left(e^{\frac{-\omega}{kT}}-1\right)^2} + A_{dir}TH^4 \quad (3)$$

Experimental

Materials and methods

All manipulations related to the synthesis of the obtained compounds were carried out in an inert atmosphere using evacuated glass ampoules. Acetonitrile was dried over P_2O_5, kept on molecular sieves (4 Å) and vacuum transferred just before the synthesis. Cobalt and lithium trimethylacetates were synthesized according to previously reported procedures.[76,77] Other reagents (2-furoic acid (2-Hfur), 3,5-di-*tert*-butylbenzoic acid (Hbzo), 3-cyanobenzoic acid (3-Hcba), 4-cyanobenzoic acid (4-Hcba), 2,2′-bypyridine (bpy), 4-phenylpyridine (4PhPy) and quinoline (quin)) are commercially available and were used as purchased.

IR spectra of the compounds were recorded on a PerkinElmer Spectrum 65 spectrophotometer equipped with a Quest ATR Accessory (Specac) by the attenuated total reflectance (ATR) in the range of 400–4000 cm^{-1}. Elemental analysis was performed on a Euro EA-3000 (Euro Vektor) automated C, H,N,S-analyzer.

The X-ray diffraction datasets for crystals of compounds **1–5** were collected on a Bruker Apex II diffractometer equipped with a CCD detector (Mo-K_α, λ = 0.71073 Å) and graphite monochromator.[78] Crystal reflection analysis of crystals of compounds **4** and **5** revealed non-merohedral twinning. The orientation matrices for the two domains were determined using the Cell Now program,[79] both components were combined using Apex3. A semi-empirical absorption correction for compounds **4** and **5** was applied using the Twinabs software.[80] For compounds **1–3** a semi-empirical absorption correction was applied using the SADABS[81] program. Using Olex2,[82] the structure was solved with a ShelXS structure solution program using direct methods and refined using a ShelXL[83] refinement package. The structures **4** and **5** were solved on the basis of unique domain 1 reflections and refined using *hkl* 5. The H-atoms were added in the calculated positions and refined using the riding model in isotropic approximation. The SHAPE 2.1 software (University of Barcelona, Barcelona, Catalonia, Spain)[84] was used to determine the metal's polyhedron geometry.

The powder X-ray diffraction patterns were obtained using the Bruker D8 Advance diffractometer with a LynxEye detector in Bragg–Brentano geometry. The sample was finely dispersed on a silicon holder with a zero background, λ(CuKα) = 1.5418 Å. The acquired data were refined using TOPAS 4 software.[85]

The magnetic measurements were done on a Quantum Design PPMS-9 with the ACMS option. The dc magnetic sus-

ceptibility measurements were carried out in the temperature range of 2–300 K in a 5000 Oe dc field. The ac magnetic fields with an amplitude of 1, 3, and 5 Oe in frequency ranges of 10 000–1000, 1000–100, 100–10 Hz, respectively, were used for measuring the ac magnetic susceptibility. These settings make it possible to both avoid sample heating at low temperatures (which can take place at high modulation amplitudes and frequencies) and obtain the best signal-to-noise ratio. The results of ac magnetic susceptibility measurements were processed using a standard procedure.[62] The measurements were performed on polycrystalline samples covered with mineral oil and sealed in polyethylene bags to prevent the orientation of crystallites under the external magnetic field. The paramagnetic component of the magnetic susceptibility (χ) was determined by taking into account the diamagnetic contribution evaluated from Pascal's constants as well as the contributions of the sample holder and mineral oil.

Ab initio (post Hartree–Fock) calculations of the ZFS parameters and the *g*-tensor were performed based on the state-averaged complete-active-space self-consistent-field (*SA-CASSCF*) wave function[86] complemented by N-electron valence second-order perturbation theory (*NEVPT2*)[87] using the ORCA program package (version 5.0.4).[88] The calculations were performed with the geometry of the experimentally determined X-ray structures. The active space of the *CASSCF* calculations was composed of seven electrons in five d-orbitals of Co^{2+} ions (S = 3/2): CAS(7,5). The state-averaged approach was used, in which all 10 quartet (S = 3/2) and 40 doublet (S = 1/2) states were averaged with equal weights. Relativistic effects were taken into account by using the second-order Douglas–Kroll–Hess Hamiltonian (DKH).[89] The polarized triple-ζ-quality DHK-def2-TZVP basis set was used for nonhydrogen atoms[90] and double-ζ-quality def2-SVP for hydrogen. An auxiliary def2/JK Coulomb fitting basis set was used in the calculation.[91] Both the zero-field splitting parameter (D) and transverse anisotropy (E), based on dominant spin–orbit coupling contributions from excited states, were calculated through the quasi-degenerate perturbation theory (*QDPT*),[92] in which approximation to the Breit–Pauli form of the spin–orbit coupling operator (*SOMF*)[93] and an effective Hamiltonian approach[94] were applied. The splitting of the d-orbitals was analysed within the *ab initio* ligand field theory (*AILFT*).[95,96] Proximity of a polyhedron to point groups was found using CHEMCRAFT software.[97] SINGLE_ANISO mode described magnetic properties based on the calculated low-lying states.[59]

Synthesis of the complexes

$[Co_2Li_2(2\text{-fur})_6(4PhPy)_2]$ (1). Weighed portions of $[Co(piv)_2]_n$ (0.26 g, 1 mmol), $[Li(piv)]_n$ (0.108 g, 1 mmol), 4PhPy (0.156 g, 1 mmol), and 2-Hfur (0.336 g, 3 mmol) were placed in a glass ampoule and degassed in a dynamic vacuum for 30 min; acetonitrile (15 ml) was condensed into the ampoule; the latter was fire-sealed and heated in an oil bath (110 °C) until all of the reactants dissolved with formation of clear violet solution (1 h). Further heating (2 h) leads to the formation of pink crystals suitable for X-ray diffraction. After cooling to RT the mother liquor was decantated and the product was washed twice with cold acetonitrile. Yield 0.46 g (83% based on $[Co(piv)_2]_n$).

Anal. calc for $C_{52}H_{36}Co_2Li_2N_2O_{18}$ (1108.57) C, 56.34; H, 3.27; N, 2.53. Found: C, 56.28; H, 3.22; N, 2.47%. IR, ν/cm^{-1}: 3130 w, 3112 w, 1683 w, 1607 s, 1580 s, 1573 s, 1563 s, 1479 s, 1409 s, 1392 s, 1371 s, 1359 vs, 1333 m, 1312 m, 1289 w, 1239 w, 1226 m, 1199 s, 1144 w, 1140 w, 1127 w, 1079 w, 1072 m, 1046 w, 1028 m, 1011 m, 933 m, 883 m, 835 m, 818 w, 809 w, 799 w, 782 s, 757 s, 748 s, 727 m, 719 m, 685 m, 666 w, 620 w, 595 m, 578 m, 557 m, 504 s, 471 m, 441 m, 437 m.

$[Co_2Li_2(2\text{-fur})_6(bpy)_2]$ (2). Weighed portions of $[Co(piv)_2]_n$ (0.26 g, 1 mmol), $[Li(piv)]_n$ (0.108 g, 1 mmol), bpy (0.156 g, 1 mmol), and 2-Hfur (0.336 g, 3 mmol) were placed in a glass ampoule and degassed in a dynamic vacuum for 30 min; acetonitrile (15 ml) was condensed into the ampoule; the latter was fire-sealed and heated in an oil bath (110 °C) until all of the reactants dissolved with formation of clear red-orange solution (1 h). Further heating (2 h) leads to the formation of red crystals suitable for X-ray diffraction. After cooling to RT the mother liquor was decantated and the product was washed twice with cold acetonitrile. Yield 0.433 g (78% based on $[Co(piv)_2]_n$).

Anal. calc for $C_{50}H_{34}Co_2Li_2N_4O_{18}$ (1110.55) C, 54.08; H, 3.09; N, 5.04. Found: C, 54.01; H, 3.04; N, 4.97%. IR, ν/cm^{-1}: 3147 w, 3117 w, 3084 w, 3036 w, 1613 m, 1602 m, 1594 s, 1564 s, 1545 m, 1480 vs, 1441 m, 1413 s, 1392 s, 1361 s, 1315 m, 1290 w, 1250 w, 1235 w, 1221 w, 1195 m, 1185 m, 1160 w, 1139 w, 1118 w, 1076 w, 1055 w, 1040 w, 1022 m, 1009 m, 977 w, 931 m, 910 w, 883 w, 843 w, 824 w, 812 m, 789 s, 780 s, 766 vs, 751 s, 736 s, 651 m, 630 w, 611 m, 595 m, 567 w, 495 w, 483 m, 468 m, 456 m, 437 m, 422 m.

$[Co_2Li_2(bzo)_6(bpy)_2]$ (3). Weighed portions of $[Co(piv)_2]_n$ (0.13 g, 0.5 mmol), $[Li(piv)]_n$ (0.054 g, 0.5 mmol), bpy (0.078 g, 0.5 mmol), and Hbzo (0.351 g, 1.5 mmol) were placed in a glass ampoule and degassed in a dynamic vacuum for 30 min; acetonitrile (15 ml) was condensed into the ampoule; the latter was fire-sealed and heated in an oil bath (110 °C) until all of the reactants dissolved with formation of clear red-orange solution (1 h). Further heating (3 h) leads to the formation of red crystals suitable for X-ray diffraction. After cooling to RT the mother liquor was decantated and the product was washed twice with cold acetonitrile. Yield 0.348 g (74% based on $[Co(piv)_2]_n$).

Anal. calc for $C_{110}H_{142}Co_2Li_2N_4O_{12}$ (1844.07) C, 71.64; H, 7.76; N, 3.04. Found: C, 71.35; H, 7.73; N, 3.03%. IR, ν/cm^{-1}: 2961 m, 2903 m, 2868 m, 1618 m, 1581 s, 1564 m, 1544 m, 1475 m, 1459 m, 1442 m, 1388 vs, 1359 s, 1314 m, 1289 m, 1249 m, 1200 w, 1156 w, 1123 w, 1100 w, 1057 w, 1022 w, 922 w, 897 m, 889 m, 825 w, 794 s, 762 s, 733 s, 704 s, 653 w, 628 w, 609 w, 584 w, 551 w, 528 w, 489 m, 479 m.

$[Co_2Li_2(3\text{-cba})_6(quin)_2]$ (4). Weighed portions of $[Co(piv)_2]_n$ (0.26 g, 1 mmol), $[Li(piv)]_n$ (0.11 g, 1 mmol), and 3-Hcba (0.44 g, 3 mmol) were placed in a glass ampoule and degassed in a dynamic vacuum for 30 min; acetonitrile (30 ml) was condensed into the ampoule. The reaction mixture was heated until all of the reactants dissolved, with formation of clear violet solu-

tion. After that quinoline (0.13 g, 1 mmol) was added. The resulting solution was concentrated under vacuum. Violet crystals suitable for X-ray diffraction were obtained. The crystals were filtered, washed with cold acetonitrile and dried in air at RT. Yield 0.49 g (78% based on $[Co(piv)_2]_n$).

Anal. calc for $C_{66}H_{38}Co_2Li_2N_8O_{12}$ (1266.80) C, 62.57; H, 3.02; N, 8.85. Found: C, 62.32; H, 3.01; N, 8.81%. IR, ν/cm^{-1}: 3069 w, 2230 m, 1858 w, 1632 vs, 1559 s, 1508 m, 1430 vs, 1371 vs, 1310 s, 1207 s, 1164 m, 1129 m, 1088 m, 996 w, 948 m, 910 m, 818 s, 764 vs, 675 vs, 599 m, 564 s, 475 vs, 410 *vs.*

$[Co_2Li_2(4\text{-cba})_6(quin)_2]\cdot 2CH_3CN$ (5). Weighed portions of $[Co(piv)_2]_n$ (0.26 g, 1 mmol), $[Li(piv)]_n$ (0.11 g, 1 mmol), and 4-Hcba (0.44 g, 3 mmol) were placed in a glass ampoule and degassed in a dynamic vacuum for 30 min; acetonitrile (30 ml) was condensed into the ampoule. The reaction mixture was heated until all of the reactants dissolved, with formation of clear violet solution. After that quinoline (0.13 g, 1 mmol) was added. The resulting solution was concentrated under vacuum. Violet crystals suitable for X-ray diffraction were obtained. The crystals were filtered, washed with cold acetonitrile and dried in air at RT. Yield 0.4 g (60% based on $[Co(piv)_2]_n$).

Anal. calc for $C_{70}H_{44}Co_2Li_2N_{10}O_{12}$ (1348.91) C, 62.33; H, 3.29; N, 10.38. Found: C, 62.08; H, 3.28; N, 10.34%. IR, ν/cm^{-1}: 3397 m, 2362 w, 2231 m, 1635 s, 1583 s, 1529 vs, 1376 vs, 1292 s, 1137 m, 1021 m, 865 m, 779 vs, 693 s, 573 vs, 539 vs, 465 vs, 409 *vs.*

Conclusions

Thus, we reported a series of tetranuclear heterometallic complexes with a $\{Co_2Li_2\}$ metal core. In compounds containing monodentate N-donor ligands (**1**, **4**, **5**), the cobalt atoms are in a distorted tetrahedral environment, while in complexes with the chelating bipyridine ligand (**2**, **3**), the cobalt atoms are in a distorted octahedral environment. According to magnetic measurements and quantum chemical calculations, compounds **1–4** exhibit an easy-plane type of anisotropy, with a positive *D* value. The slow relaxation of magnetization in complexes **1–3** occurs through a combination of Raman and direct relaxation mechanisms. The obtained results are similar to those previously described for complexes with a $\{Co_2Li_2\}$ metal core.[49–51] However, in compound **4**, the Orbach relaxation mechanism may contribute to the slow relaxation of magnetization. Furthermore, the relaxation process in **4** could be described by the vibrational process and direct mechanism.

Author contributions

Conceptualization: Stanislav A. Nikolaevskii and Mikhail A. Kiskin; investigation: Irina K. Rubtsova, Dmitriy S. Yambulatov, Maxim A. Shmelev, Julia K. Voronina, Alexander S. Goloveshkin, and Konstantin A. Babeshkin; formal analysis: Irina K. Rubtsova, Nikolay N. Efimov, and Anna K. Matiukhina; writing – original draft: Irina K. Rubtsova, Maxim A. Shmelev, Nikolay N. Efimov, Anna K. Matiukhina, and Stanislav A. Nikolaevskii; writing – review and editing: Mikhail A. Kiskin and Igor L. Eremenko; funding acquisition and supervision: Igor L. Eremenko.

Conflicts of interest

The authors of this work declare that they have no conflicts of interest.

Data availability

The data supporting this article have been included as part of the supplementary information (SI). Supplementary information is available. See DOI: https://doi.org/10.1039/d5dt02560e.

CCDC 2340654 (**1**), 2340655 (**2**), 2340656 (**3**), 2340657 (**4**) and 2340658 (**5**) contain the supplementary crystallographic data for this paper.[98a–e]

Acknowledgements

This work was supported by the Ministry of Science and Higher Education of the Russian Federation as part of the State Assignment of the Kurnakov Institute of General and Inorganic Chemistry of the Russian Academy of Sciences.

This research was performed using the equipment of the JRC PMR IGIC RAS (X-ray diffraction, CHN and IR-spectral analyses, magnetochemical measurements).

The Center for Molecular Composition Studies at INEOS RAS (Powder XRD with Rietveld refinement), which operates with the support of the state assignment of the INEOS RAS in the field of fundamental scientific research, is gratefully acknowledged.

References

1 G. A. Craig and M. Murrie, *Chem. Soc. Rev.*, 2015, **44**, 2135–2147.
2 L. Rosado Piquer and E. C. Sañudo, *Dalton Trans.*, 2015, **44**, 8771–8780.
3 J. Wang, M. Feng, M. N. Akhtar and M.-L. Tong, *Coord. Chem. Rev.*, 2019, **387**, 129–153.
4 A. Dey, J. Acharya and V. Chandrasekhar, *Chem. – Asian J.*, 2019, **14**, 4433–4453.
5 D. Shao and X. Wang, *Chin. J. Chem.*, 2020, **38**, 1005–1018.
6 V. S. Parmar, D. P. Mills and R. E. P. Winpenny, *Chem. – Eur. J.*, 2021, **27**, 7625–7645.
7 V. V. Novikov and Y. V. Nelyubina, *Russ. Chem. Rev.*, 2021, **90**, 1330–1358.
8 D. P. DiVincenzo, *Fortschr. Phys.*, 2000, **48**, 771–783.
9 V. I. Minkin, *Russ. Chem. Bull.*, 2008, **57**, 687–717.
10 V. V. Novikov, A. A. Pavlov, Y. V. Nelyubina, M.-E. Boulon, O. A. Varzatskii, Y. Z. Voloshin and R. E. P. Winpenny, *J. Am. Chem. Soc.*, 2015, **137**, 9792–9795.

11 P. Zhang, Q. Luo, Z. Zhu, W. He, N. Song, J. Lv, X. Wang, Q. Zhai, Y. Zheng and J. Tang, *Angew. Chem., Int. Ed.*, 2023, **62**, e202218540.
12 M. Murrie, *Chem. Soc. Rev.*, 2010, **39**, 1986.
13 P. Kumar Sahu, R. Kharel, S. Shome, S. Goswami and S. Konar, *Coord. Chem. Rev.*, 2023, **475**, 214871.
14 X.-N. Yao, J.-Z. Du, Y.-Q. Zhang, X.-B. Leng, M.-W. Yang, S.-D. Jiang, Z.-X. Wang, Z.-W. Ouyang, L. Deng, B.-W. Wang and S. Gao, *J. Am. Chem. Soc.*, 2017, **139**, 373–380.
15 P. C. Bunting, M. Atanasov, E. Damgaard-Møller, M. Perfetti, I. Crassee, M. Orlita, J. Overgaard, J. Van Slageren, F. Neese and J. R. Long, *Science*, 2018, **362**, eaat7319.
16 J. Du, W. Chen, Q. Chen, X. Leng, Y.-S. Meng, S. Gao and L. Deng, *Organometallics*, 2020, **39**, 729–739.
17 K. C. Mondal, S. Roy, S. De, P. Parameswaran, B. Dittrich, F. Ehret, W. Kaim and H. W. Roesky, *Chem. – Eur. J.*, 2014, **20**, 11646–11649.
18 J. Du, L. Wang, M. Xie and L. Deng, *Angew. Chem., Int. Ed.*, 2015, **54**, 12640–12644.
19 T. R. Dugan, X. Sun, E. V. Rybak-Akimova, O. Olatunji-Ojo, T. R. Cundari and P. L. Holland, *J. Am. Chem. Soc.*, 2011, **133**, 12418–12421.
20 A. S. Zaguzin, P. A. Abramov, M. I. Rakhmanova, A. N. Usoltsev, M. N. Sokolov, V. P. Fedin and S. A. Adonin, *Polyhedron*, 2024, **253**, 116908.
21 A. S. Zaguzin, M. A. Bondarenko, P. A. Abramov, M. I. Rakhmanova, M. N. Sokolov, V. P. Fedin and S. A. Adonin, *Inorganics*, 2022, **10**, 262.
22 M. A. Bondarenko, M. I. Rakhmanova, A. S. Novikov, M. N. Sokolov and S. A. Adonin, *Mendeleev Commun.*, 2022, **32**, 585–587.
23 M. A. Bondarenko, P. A. Abramov, I. V. Korolkov, A. S. Bogomyakov, M. N. Sokolov and S. A. Adonin, *CrystEngComm*, 2023, **25**, 130–136.
24 Z.-B. Xie, T.-C. Yue, Q.-W. Dong, Q.-C. Ma, Q.-W. Cao, L.-L. Wang and D.-Z. Wang, *Polyhedron*, 2024, **249**, 116777.
25 Q. Zhang, S.-Y. Yang, S.-J. Chen, L. Shi, J. Yang, Z. Tian, Z. Ruan and D. Shao, *J. Mol. Struct.*, 2023, **1294**, 136349.
26 A. Nikiforov, N. Panina, D. Blinou, V. Gurzhiy, J. Nashchekina, E. Korzhikova-Vlakh, A. Eremin and M. Stepanova, *Catalysts*, 2023, **13**, 304.
27 M. Zeng, M. Yao, H. Liang, W. Zhang and X. Chen, *Angew. Chem., Int. Ed.*, 2007, **46**, 1832–1835.
28 K. W. Galloway, A. M. Whyte, W. Wernsdorfer, J. Sanchez-Benitez, K. V. Kamenev, A. Parkin, R. D. Peacock and M. Murrie, *Inorg. Chem.*, 2008, **47**, 7438–7442.
29 J. Acharya, A. Swain, A. Chakraborty, V. Kumar, P. Kumar, J. F. Gonzalez, O. Cador, F. Pointillart, G. Rajaraman and V. Chandrasekhar, *Inorg. Chem.*, 2019, **58**, 10725–10735.
30 A. Topor, D. Liu, C. Maxim, G. Novitchi, C. Train, Z. A. AlOthman, A. A. S. Al-Kahtani, L. Ungur, L. T. A. Ho, L. F. Chibotaru and M. Andruh, *J. Mater. Chem. C*, 2021, **9**, 10912–10926.
31 Z.-W. An, Y.-Q. Gao, S.-M. Xu, W. Zhang and M.-X. Yao, *Cryst. Growth Des.*, 2023, **23**, 1412–1421.
32 A. Zabala-Lekuona, X. Lopez De Pariza, I. F. Díaz-Ortega, J. Cepeda, H. Nojiri, N. P. Gritsan, A. A. Dmitriev, A. López-Ortega, A. Rodríguez-Diéguez, J. M. Seco and E. Colacio, *Dalton Trans.*, 2024, **53**, 7971–7984.
33 D. Dermitzaki, C. P. Raptopoulou, V. Psycharis, A. Escuer, S. P. Perlepes, J. Mayans and T. C. Stamatatos, *Dalton Trans.*, 2021, **50**, 240–251.
34 M. A. Palacios, S. Titos-Padilla, J. Ruiz, J. M. Herrera, S. J. A. Pope, E. K. Brechin and E. Colacio, *Inorg. Chem.*, 2014, **53**, 1465–1474.
35 M. Biswas, E. C. Sañudo and D. Ray, *Inorg. Chem.*, 2021, **60**, 11129–11139.
36 S. A. Nikolaevskii, D. S. Yambulatov, J. K. Voronina, S. N. Melnikov, K. A. Babeshkin, N. N. Efimov, A. S. Goloveshkin, M. A. Kiskin, A. A. Sidorov and I. L. Eremenko, *ChemistrySelect*, 2020, **5**, 12829–12834.
37 A. A. Sidorov, N. V. Gogoleva, E. S. Bazhina, S. A. Nikolaevskii, M. A. Shmelev, E. N. Zorina-Tikhonova, A. G. Starikov, M. A. Kiskin and I. L. Eremenko, *Pure Appl. Chem.*, 2020, **92**, 1093–1110.
38 T. S. Bennett, N. Geue, G. A. Timco, G. F. S. Whitehead, I. J. Vitorica-Yrezabal, P. E. Barran, E. J. L. McInnes and R. E. P. Winpenny, *Chem. – Eur. J.*, 2024, **30**, e202400432.
39 M. Darii, J. Van Leusen, V. C. Kravtsov, Y. Chumakov, K. Krämer, S. Decurtins, S.-X. Liu, P. Kögerler and S. G. Baca, *Cryst. Growth Des.*, 2023, **23**, 6944–6952.
40 I. A. Lutsenko, M. A. Kiskin, S. A. Nikolaevskii, A. A. Starikova, N. N. Efimov, A. V. Khoroshilov, A. S. Bogomyakov, I. V. Ananyev, J. K. Voronina, A. S. Goloveshkin, A. A. Sidorov and I. L. Eremenko, *ChemistrySelect*, 2019, **4**, 14261–14270.
41 I. K. Rubtsova, S. A. Nikolaevskii, I. L. Eremenko and M. A. Kiskin, *Russ. J. Coord. Chem.*, 2023, **49**, 695–709.
42 N. Ishikawa, M. Sugita, T. Ishikawa, S. Koshihara and Y. Kaizu, *J. Am. Chem. Soc.*, 2003, **125**, 8694–8695.
43 N. Ishikawa, M. Sugita, T. Ishikawa, S. Koshihara and Y. Kaizu, *J. Phys. Chem. B*, 2004, **108**, 11265–11271.
44 S. Demir, I.-R. Jeon, J. R. Long and T. D. Harris, *Coord. Chem. Rev.*, 2015, **289–290**, 149–176.
45 J. Nehrkorn, I. A. Valuev, M. A. Kiskin, A. S. Bogomyakov, E. A. Suturina, A. M. Sheveleva, V. I. Ovcharenko, K. Holldack, C. Herrmann, M. V. Fedin, A. Schnegg and S. L. Veber, *J. Mater. Chem. C*, 2021, **9**, 9446–9452.
46 J. Kobylarczyk, M. Liberka, P. Konieczny, S. Baran, M. Kubicki, T. Korzeniak and R. Podgajny, *Dalton Trans.*, 2020, **49**, 300–311.
47 M. Soler, W. Wernsdorfer, K. Folting, M. Pink and G. Christou, *J. Am. Chem. Soc.*, 2004, **126**, 2156–2165.
48 E.-C. Yang, W. Wernsdorfer, L. N. Zakharov, Y. Karaki, A. Yamaguchi, R. M. Isidro, G.-D. Lu, S. A. Wilson, A. L. Rheingold, H. Ishimoto and D. N. Hendrickson, *Inorg. Chem.*, 2006, **45**, 529–546.
49 D. S. Yambulatov, S. A. Nikolaevskii, M. A. Shmelev, K. A. Babeshkin, D. V. Korchagin, N. N. Efimov, A. S. Goloveshkin, P. A. Petrov, M. A. Kiskin, M. N. Sokolov and I. L. Eremenko, *Mendeleev Commun.*, 2021, **31**, 624–627.

50 D. S. Yambulatov, S. A. Nikolaevskii, A. N. Lukoyanov, M. A. Shmelev, J. K. Voronina, K. A. Babeshkin, A. K. Matiukhina, N. N. Efimov, M. A. Kiskin and I. L. Eremenko, *New J. Chem.*, 2023, **47**, 19362–19366.
51 I. K. Rubtsova, P. N. Vasilyev, J. K. Voronina, M. A. Shmelev, N. N. Efimov, S. A. Nikolaevskii, I. L. Eremenko and M. A. Kiskin, *Russ. J. Coord. Chem.*, 2024, **50**, 523–533.
52 P. Halaš, I. Nemec, E. Čižmár and R. Herchel, *Dalton Trans.*, 2025, **54**, 10140–10149.
53 P. Halaš, I. Nemec and R. Herchel, *Magnetochemistry*, 2023, **9**, 229.
54 N. F. Chilton, R. P. Anderson, L. D. Turner, A. Soncini and K. S. Murray, *J. Comput. Chem.*, 2013, **34**, 1164–1175.
55 A. K. Matiukhina, E. N. Zorina-Tikhonova, D. O. Blinou, R. D. Svetogorov, P. N. Vasilyev, N. N. Efimov, M. A. Kiskin and I. L. Eremenko, *J. Magn. Magn. Mater.*, 2025, **614**, 172650.
56 D. Schweinfurth, M. G. Sommer, M. Atanasov, S. Demeshko, S. Hohloch, F. Meyer, F. Neese and B. Sarkar, *J. Am. Chem. Soc.*, 2015, **137**, 1993–2005.
57 J. Vallejo, I. Castro, R. Ruiz-García, J. Cano, M. Julve, F. Lloret, G. De Munno, W. Wernsdorfer and E. Pardo, *J. Am. Chem. Soc.*, 2012, **134**, 15704–15707.
58 R. Boča, C. Rajnák and J. Titiš, *Magnetochemistry*, 2023, **9**, 100.
59 L. F. Chibotaru and L. Ungur, *J. Chem. Phys.*, 2012, **137**, 064112.
60 S. Gómez-Coca, A. Urtizberea, E. Cremades, P. J. Alonso, A. Camón, E. Ruiz and F. Luis, *Nat. Commun.*, 2014, **5**, 4300.
61 C. E. Jackson, I. P. Moseley, R. Martinez, S. Sung and J. M. Zadrozny, *Chem. Soc. Rev.*, 2021, **50**, 6684–6699.
62 N. N. Efimov, K. A. Babeshkin and A. V. Rotov, *Russ. J. Coord. Chem.*, 2024, **50**, 363–373.
63 Y.-Q. Zhai and Y.-Z. Zheng, *J. Mater. Chem. C*, 2021, **9**, 8096–8098.
64 A. Lunghi, F. Totti, S. Sanvito and R. Sessoli, *Chem. Sci.*, 2017, **8**, 6051–6059.
65 L. Escalera-Moreno, J. J. Baldoví, A. Gaita-Ariño and E. Coronado, *Chem. Sci.*, 2018, **9**, 3265–3275.
66 J. Torrent, C. Puigjaner, R. Herchel and J. Mayans, *Inorg. Chem.*, 2025, **64**, 3735–3746.
67 L. Gu and R. Wu, *Phys. Rev. Lett.*, 2020, **125**, 117203.
68 A. Lunghi, F. Totti, R. Sessoli and S. Sanvito, *Nat. Commun.*, 2017, **8**, 14620.
69 K.-X. Yu, J. G. C. Kragskow, Y.-S. Ding, Y.-Q. Zhai, D. Reta, N. F. Chilton and Y.-Z. Zheng, *Chem*, 2020, **6**, 1777–1793.
70 Y. Ma, Y. Zhai, Q. Luo, Y. Ding and Y. Zheng, *Angew. Chem., Int. Ed.*, 2022, **61**, e202206022.
71 B.-K. Ling, Y.-Q. Zhai, P.-B. Jin, H.-F. Ding, X.-F. Zhang, Y. Lv, Z. Fu, J. Deng, M. Schulze, W. Wernsdorfer and Y.-Z. Zheng, *Matter*, 2022, **5**, 3485–3498.
72 L. Gu, J. Luo, Q. Luo, Y. Zhai, Y.-Z. Zheng and G. Zhao, *Chin. Phys. Lett.*, 2025, **42**, 027401.
73 Q.-C. Luo and Y.-Z. Zheng, *Trends Chem.*, 2023, **5**, 869–872.
74 A. Lunghi and S. Sanvito, *J. Chem. Phys.*, 2020, **153**, 174113.
75 S. Mondal and A. Lunghi, *J. Am. Chem. Soc.*, 2022, **144**, 22965–22975.
76 I. G. Fomina, G. G. Aleksandrov, Zh. V. Dobrokhotova, O. Y. Proshenkina, M. A. Kiskin, Y. A. Velikodnyi, V. N. Ikorskii, V. M. Novotortsev and I. L. Eremenko, *Russ. Chem. Bull.*, 2006, **55**, 1909–1919.
77 E. N. Zorina-Tikhonova, D. S. Yambulatov, M. A. Kiskin, E. S. Bazhina, S. A. Nikolaevskii, N. V. Gogoleva, I. A. Lutsenko, A. A. Sidorov and I. L. Eremenko, *Russ. J. Coord. Chem.*, 2020, **46**, 75–80.
78 *Apex3*, Bruker AXS Inc., Madison, Wisconsin, USA, 2016.
79 G. M. Sheldrick, *Cell_Now*, Bruker AXS Inc., Madison, Wisconsin, USA, 2004.
80 *Twinabs*, Bruker AXS Inc., Madison, Wisconsin, USA, 2001.
81 G. M. Sheldrick, *SADABS*, Bruker AXS Inc., Madison, Wisconsin, USA, 1997.
82 O. V. Dolomanov, L. J. Bourhis, R. J. Gildea, J. A. K. Howard and H. Puschmann, *J. Appl. Crystallogr.*, 2009, **42**, 339–341.
83 G. M. Sheldrick, *Acta Crystallogr., Sect. A:Found. Adv.*, 2015, **71**, 3–8.
84 M. Llunell, D. Casanova, J. Cirera, P. Alemany and S. Alvarez, *SHAPE (version 2.1)*, 2013.
85 N. V. Y. Scarlett and I. C. Madsen, *Powder Diffr.*, 2006, **21**, 278–284.
86 P.-Å. Malmqvist and B. O. Roos, *Chem. Phys. Lett.*, 1989, **155**, 189–194.
87 C. Angeli, R. Cimiraglia, S. Evangelisti, T. Leininger and J.-P. Malrieu, *J. Chem. Phys.*, 2001, **114**, 10252–10264.
88 F. Neese, *Wiley Interdiscip. Rev.: Comput. Mol. Sci.*, 2012, **2**, 73–78.
89 A. Wolf, M. Reiher and B. A. Hess, *J. Chem. Phys.*, 2002, **117**, 9215–9226.
90 A. Schäfer, C. Huber and R. Ahlrichs, *J. Chem. Phys.*, 1994, **100**, 5829–5835.
91 F. Neese, *J. Comput. Chem.*, 2003, **24**, 1740–1747.
92 D. Ganyushin and F. Neese, *J. Chem. Phys.*, 2006, **125**, 024103.
93 F. Neese, *J. Chem. Phys.*, 2005, **122**, 034107.
94 R. Maurice, R. Bastardis, C. D. Graaf, N. Suaud, T. Mallah and N. Guihéry, *J. Chem. Theory Comput.*, 2009, **5**, 2977–2984.
95 *Molecular Electronic Structures of Transition Metal Complexes II*, ed. D. M. P. Mingos, P. Day and J. P. Dahl, Springer Berlin Heidelberg, Berlin, Heidelberg, 2012, vol. 143.
96 S. K. Singh, J. Eng, M. Atanasov and F. Neese, *Coord. Chem. Rev.*, 2017, **344**, 2–25.
97 Chemcraft – graphical software for visualization of quantum chemistry computations (version 1.8, build 682), https://www.chemcraftprog.com.
98 (*a*) CCDC 2340654: Experimental Crystal Structure Determination, 2026, DOI: 10.5517/ccdc.csd.cc2jkmzq; (*b*) CCDC 2340655: Experimental Crystal Structure Determination, 2026, DOI: 10.5517/ccdc.csd.cc2jkn0s; (*c*) CCDC 2340656: Experimental Crystal Structure Determination, 2026, DOI: 10.5517/ccdc.csd.cc2jkn1t; (*d*) CCDC 2340657: Experimental Crystal Structure Determination, 2026, DOI: 10.5517/ccdc.csd.cc2jkn2v; (*e*) CCDC 2340658: Experimental Crystal Structure Determination, 2026, DOI: 10.5517/ccdc.csd.cc2jkn3w.